## Coulomb-Engineered Topology

M. Rösner<sup>1</sup> and J. L. Lado<sup>2</sup>

<sup>1</sup>Radboud University, Institute for Molecules and Materials, NL-6525 AJ Nijmegen, the Netherlands

<sup>2</sup>Department of Applied Physics, Aalto University, 00076 Aalto, Espoo, Finland

(Dated: April 10, 2022)

The interplay of topology and interactions is at the heart of current condensed matter research. In particular, intensive efforts are being directed towards engineering artificial systems displaying topological excitations. Most of these efforts focus on single-particle properties neglecting possible engineering routes via the modifications to the fundamental many-body interactions. Here we propose a simple platform in which topologically non-trivial many-body states emerge solely from dielectrically-engineered Coulomb interactions in an otherwise topologically trivial single-particle band structure. We demonstrate how our proposal can be realized in one-dimensional systems, such as quantum-dot chains, by exploiting Coulomb engineering, which has recently been applied to a variety of two-dimensional materials. Our results put forward Coulomb engineering as a powerful tool to create topological states of matter, with potential applications in a variety of solid-state platforms.

Topology represents one of the most fertile fields in modern condensed matter physics, [1-3] boosted by the prediction and experimental realization of topological insulators, ranging from quantum spin Hall insulators, [4] to Chern insulators, topological superconductors, [5-7] and topological crystalline insulators.[8, 9] Besides their fundamental interest, these states are nowadays widely discussed due to their potential impact to solid-state technology, including low consumption electronics, [10] spintronics[11] and topological quantum computing.[12] The topological classification of non-interacting systems continues to grow in recent years, with the recent examples of higher order topological insulators, [13, 14] non-Hermitian topology, [15–17] fragile topological phases, [18, 19] quasi-periodic topology[20, 21] and random topological systems. [22, 23] Remarkably, all these unconventional states stem from single-particle phenomena, relying only on properly engineered free-particle Hamiltonians.

Some of the most ground-breaking discoveries in condensed matter physics have been intimately related with strong interactions, with the paradigmatic examples of high-temperature superconductivity[24] and fractional quantum Hall physics.[25, 26] Thus, it is not surprising that the interplay of topology and correlation effects is raising as one of the most enigmatic fields in modern condensed matter physics. Topological states associated to interactions in topological Mott insulators[27] and Kondo insulators[28, 29] represent first examples in this context. In many instances, the role of interactions in generating topology is reduced to a mean-field single-particle effect.[27–30] However, the potential genuine role of interactions in topological systems, going beyond mean-field single particle effects is still at a very early stage.

Here, we demonstrate that Coulomb-engineered local interactions allow to induce a many-body topological state of matter. Our mechanism puts forward a paradigm to generate topological states purely driven by electronic interactions without relying on conventional

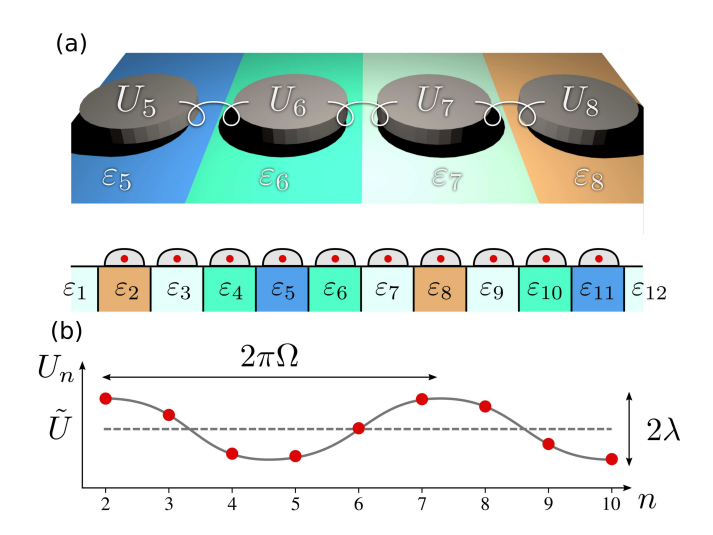


FIG. 1. (a) Sketch of the proposed system: a linear chain of quantum dots is deposited on a substrate that modulates the local electronic interactions. The spatial modulation of the substrate permitivity results in a spatially dependent environmental screening, giving rise to site-dependent local Coulomb interactions within the otherwise homogeneous quantum-dot chain (b).

single-particle properties. Ultimately, we demonstrate that this procedure allows to generate topological states of matter that cannot be captured at the mean-field electronic level, yielding a genuine many-body topological state. These topological states result from imprinting quasi-periodic structures to the local Coulomb interactions  $U_n$  only, without requiring modifications to the topologically trivial single-particle dispersions. We show how such a spatial structuring of the local interactions can be achieved in experimentally realistic setups based on quantum-dot arrays and by exploiting Coulomb engineering[31–34] via structuring the substrate, as depicted in Fig. 1.

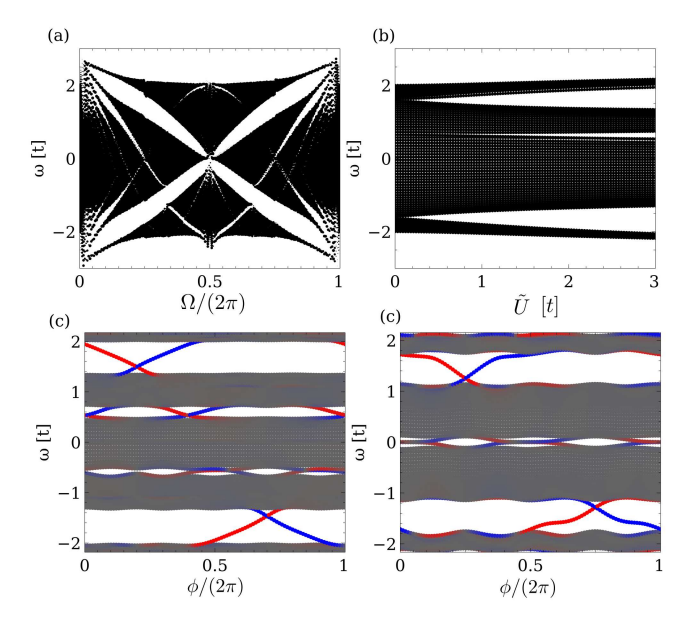


FIG. 2. Screening-induced mean-field topology: (a) Bulk spectra as a function of the modulation frequency  $\Omega$ , and evolution of the spectra as a function of  $\tilde{U}$  (b). (c,d) Full spectra as a function of the pumping parameter  $\phi$  for  $\Omega=0.4\pi$  (c) and  $\Omega=0.5\pi$  (d). Panel (a) shows the emergence of topological gaps, and panel (b) shows the emergence edge states pumping through the gap. Red/blue denotes left/right edge, the Fermi level is at E=0.0 and the system half filled. We choose  $\tilde{U}=6t,\ \lambda=0.5$  in (a,c,d), a chain length of 80 sites in (a-d), and  $\Omega=0.4\pi$  in (b).

Screening-Induced Single-Particle Topology: To exemplify our proposal, we start with a model in which interactions generate a topological state that can be understood on the single-particle level within a mean-field framework. To this end, we consider a linear array of quantum dots (QDs) with a single level per dot and spatially modulated local Coulomb interactions. The corresponding Hamiltonian reads

$$H = \sum_{n,s} t \, c_{n,s}^{\dagger} c_{n+1,s} + \sum_{n} U_n \, c_{n,\uparrow}^{\dagger} c_{n,\uparrow} c_{n,\downarrow}^{\dagger} c_{n,\downarrow}, \qquad (1)$$

where n is the QD site index, t the hopping amplitude between neighbouring QDs and  $U_n$  a spatially varying local Coulomb repulsion of the form

$$U_n = \tilde{U}[1 + \lambda \cos(\Omega n + \phi)], \tag{2}$$

which is periodically modulated around a constant U.  $\Omega$ ,  $\phi$ , and  $\lambda$  are the modulation wavelength, phase, and strength, respectively, which can be effectively controlled by means of Coulomb engineering via spatially structured substrates as we demonstrate later in the manuscript. With these parameters, we are able to explore the full phase space of possible Coulomb pattern-induced topological effects. We solve this model via a mean field decoupling leading to the mean-field Hamiltonian H

 $\sum_{n,s} c_{n,s}^{\dagger} c_{n+1,s} + \sum_{n} U_n \langle c_{n,s}^{\dagger} c_{n,s} \rangle c_{n,\bar{s}}^{\dagger} c_{n,\bar{s}}$ . Assuming time reversal symmetry, i.e.  $\langle c_{n,\uparrow}^{\dagger} c_{n,\uparrow} \rangle = \langle c_{n,\downarrow}^{\dagger} c_{n,\downarrow} \rangle$ , the interactions  $U_n$  locally renormalize the onsite energies, following the modulation profile defined in Eq. 2. This mean-field Hamiltonian is of the same form as a diagonal Aubry-Andre-Harper model[35, 36] for electrons with a non-zero charge average per site, that is known to have edge states stemming from a parent two-dimensional Hall state[37, 38]. In Fig. 1 a) we show the full bulk energy spectrum of a QD chain with 80 sites as a function of  $\Omega$  at half-filling and using U = 6t and  $\lambda = 0.5$ , which is clearly gapped in certain regions. As shown in Fig. 1 b) for  $\Omega = 0.4\pi$ , those gaps increase as U is ramped up. These gaps are of topological origin, [39] as depicted in Figs. 2 c) and d), where we show the mean-field spectrum as a function of  $\phi$  for  $\Omega = 0.4\pi$  and  $\Omega = 0.6\pi$ . In particular, we see two edge modes (red/blue) that cross the gap as  $\phi$  is changed. Those states are topological modes of the system, and stem from the non-trivial topological invariant of the single-particle band-structure.[39] Thus, the spatially modulated onsite Hubbard interactions are capable of generating topological non-trivial edge modes by modulating the effective single-particle mean-field Hamiltonian. While this is a rather simple mechanism on the effective single-particle level, it exemplifies that interactions alone are able to induce non-trivial topology.

Screening-Induced Many-Body Topology: Another more sophisticated scenario refers to the possibility to induce non-trivial topological behaviour via dielectric engineering in a regime with a topologically trivial mean-field Hamiltonian. To this end, we propose a similar interacting Hamiltonian as before, but with exactly one electron per site:

$$H = \sum_{n,s} t \, c_{n,s}^{\dagger} c_{n+1,s}$$

$$+ \sum_{n} U_n \left( c_{n,\uparrow}^{\dagger} c_{n,\uparrow} - \frac{1}{2} \right) \left( c_{n,\downarrow}^{\dagger} c_{n,\downarrow} - \frac{1}{2} \right).$$

$$(3)$$

This Hamiltonian can be understood as a non-uniform Hubbard QD chain, in which each QD is biased so that it is half filled. The corresponding mean-field decoupled Hamiltonian is by construction uniform  $H_{mf} =$  $\sum_{n,s} t c_{n,s}^{\dagger} c_{n+1,s}$  and thus topologically trivial. To exactly solve the interacting many-body problem defined by the Hamiltonian in Eq. 3, we use the tensor network formalism. For all  $\phi$  the system remains non-magnetic and half filled in every site  $\langle n \rangle = 1$ . In the following we analyze the dynamical spin response  $S(\omega, n)$  defined by  $S(\omega, n) = \langle GS | S_n^z \delta(\omega - H + E_{GS}) S_n^z | GS \rangle$ , that can be measured with inelastic spectroscopy. [40] The resulting spin responses at an edge of a chain with 30 sites are shown in Figs. 3 a) and c) as a function of  $\phi$  for different  $\Omega$ . In both situations we find modes pumping through bulk excitation gaps. The latter are visible in the bulk spin responses shown in Figs. 3 b) and d). These finite

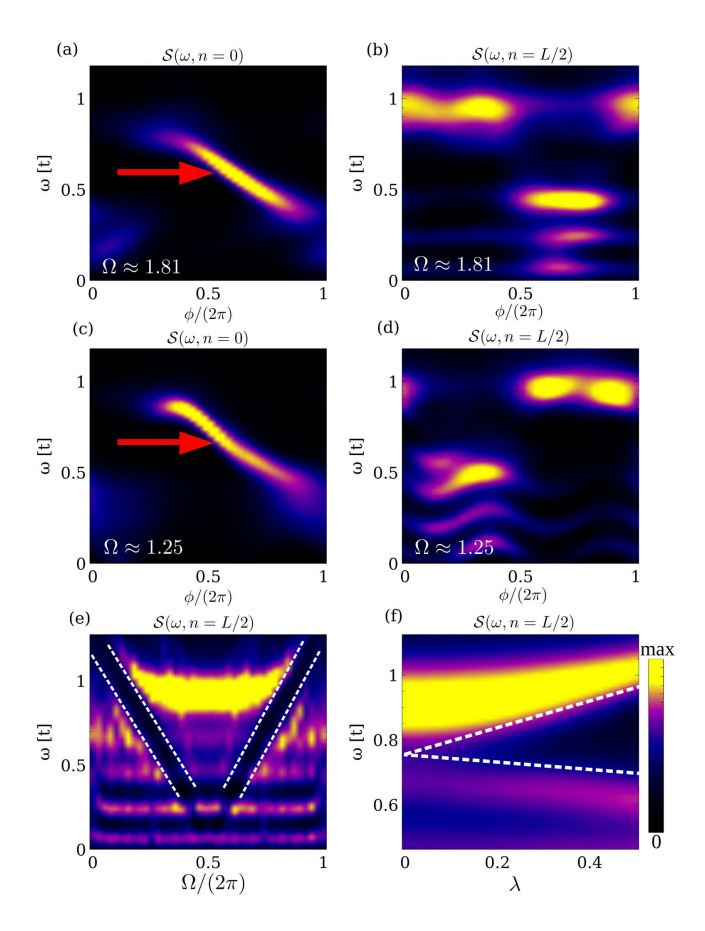


FIG. 3. Screening-induced many-body topology: spin spectral function in the edge (a) and in the bulk (b) for  $\Omega = \pi/\sqrt{3}$ . Spectral function in the edge (c) and in the bulk (d) for  $\Omega = \pi/2$ . (e) Bulk spectral function as a function of  $\Omega$ , showing gaps at generic values of  $\Omega$ . (f) Scaling of the topological gap as a function of  $\lambda$ , showing an approximate linear scaling. We took  $\lambda = 0.5$  in (a-e) and  $\tilde{U} = 6t$  (a-f) and  $\Omega = 0.4\pi$  in (f).

spectral gaps are present for arbitrary modulation frequencies  $\Omega$ , as depicted in Fig. 3 e), leading to in-gap edge excitations for generic  $\Omega$ . In particular, the gap in the bulk spin-spectral function is proportional to the Hubbard modulation strength  $\lambda$ , as shown in Fig. 3 f). We verified that such in-gap edge modes are robust towards the presence of random disorder in the modulated local Coulomb interaction  $U_n$  or second neighbor interdot hopping t'.

Many-body Origin of the Topological States: The model of Eq. 3 is a many-body version of the Aubry-Andre-Harper model as introduced in the previous section. However, a mapping to the parent electronic two-dimensional quantum Hall state cannot be performed due to its genuine many-body nature. To anyway understand how the engineered interactions are capable of creating topological edge modes here, we explore the model in the strong coupling limit, i.e.  $\tilde{U} \gg t$ . In this strongly interacting limit, spin and charge degrees of freedom are

separated while every QD is still hosting one electron, giving rise to gaped charge excitations decoupled from the spin sector. This can be explicitly shown by performing a Schrieffer-Wolff transformation of the Hamiltonian from Eq. 3 into spin operators yielding the effective Hamiltonian  $H^{eff} = \sum_{n} J_{n,n+1} \mathbf{S_n} \cdot \mathbf{S_{n+1}}$ , where  $\mathbf{S_n}$  are the S = 1/2 operators on each site, and  $J_{n,n+1}$ is the effective exchange interaction that takes the form  $J_{n,n+1} = 2t^2 \left(\frac{1}{U_n} + \frac{1}{U_{n+1}}\right) \approx \frac{4t^2}{\tilde{U}}[1 - \lambda\cos\left(\Omega n + \phi\right)].$  [41] This Hamiltonian realizes a quasi-periodic antiferromagnetic S = 1/2 Heisenberg model, [42, 43] whose ground state is a time-reversal symmetric singlet state. Such a ground state is an entangled many-body state that cannot be described as a classical symmetry broken anti-ferromagnetic state due to strong quantum fluctuations. Its low-energy excitations have S = 1/2, in contrast to S=1 of classical magnets. A common approach to characterize these low-energy excitations is to use a so-called parton Abrikosov fermion transformation of the form  $S_n^{\alpha} = \sum_{s,s'} \frac{1}{2} \sigma_{s,s'}^{\alpha} f_{n,s}^{\dagger} f_{n,s}$ , where  $f_{n,s}^{\dagger}$  and  $f_{n,s}$  are the creation and annihilation spinon operators.[44] Using this to transform the operators in  $H^{eff}$  followed by a mean-field decoupling for the Abrokosov fermions, we obtain an effective Hamiltonian of the form  $H_P^{eff}$  $\sum_{n,s} \gamma_{n,n+1} f_{n,s}^{\dagger} f_{n,s}$ .[45] This effective Hamiltonian  $H_P^{eff}$  describes fractionalized particles with S=1/2 and no charge, where the effective hoppings are proportional to the exchange coupling of the parent Heisenberg model, i.e.  $\gamma_{n,n+1} \sim J_{n,n+1}$ .  $H_P^{eff}$  thus again resembles an off-diagonal spinon Aubry-Andre-Harper model, that can be mapped to a two-dimensional quantum Hall state for spinons. As a result, the effective Hamiltonian  $H^{eff}$ hosts non-trivial edge excitations, and so does the original Hamiltonian from Eq. 3 in the strong-coupling limit, resulting from the spatially patterned local interactions.

Local Coulomb Engineering: After establishing the concept of Coulomb-engineered topology in 1D systems, we now turn to the question about its feasibility. While 1D tight-binding like chains have been regularly created, analysed, and studied in the past using, e.g., metallic nano spheres [46, 47], quantum dots [48, 49], and even single atoms [50, 51], spatially pattered Hubbard models with local Coulomb interactions of the form defined in Eq. 2 have not been created yet. Thus, we will focus in the following on how this structure of  $U_n$  can be achieved using substrate-screening effects.

The local Coulomb interactions used in the Hubbard models from above are (partially screened) Coulomb operator matrix elements evaluated in a single-orbital Wannier basis  $\psi(r)$  given by  $U_n = \int \int dr \, dr' \, |\psi(r-r_n)|^2 |\psi(r'-r_n)|^2 \, U(r,r')$ . In the following, we will approximate these elements by  $U_n \approx e\Phi_n(\vec{\delta})$ , where  $\Phi_n(\vec{x})$  is the classical electrostatic potential of an electron (point charge) with charge e localized at the Wannier state n felt by a second electron in its close vicinity at distance

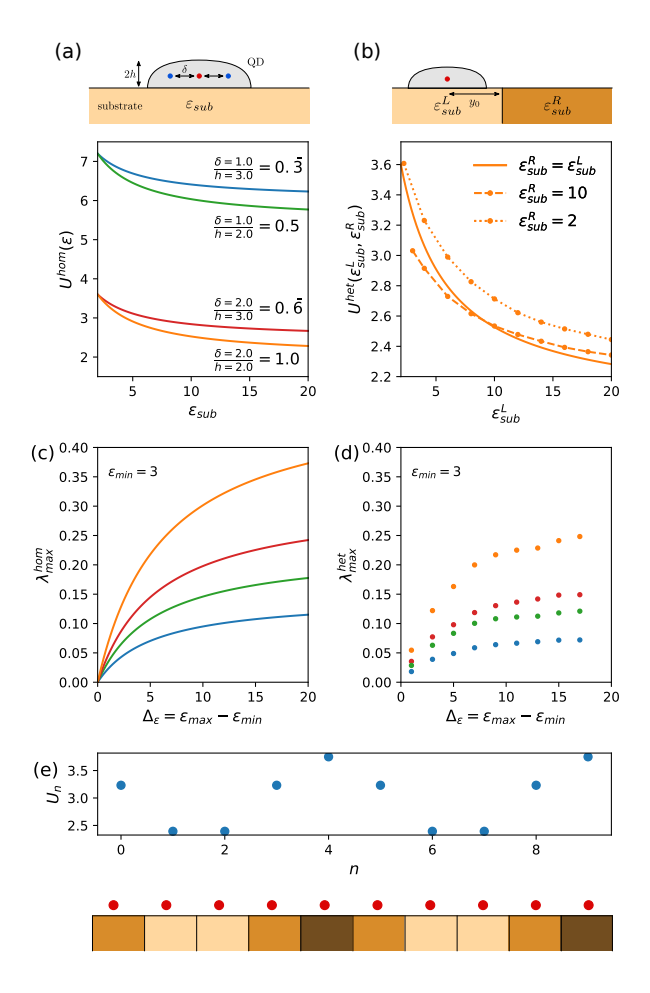


FIG. 4. Local Coulomb engineering. Local Coulomb interaction  $U_n$  controlled by (a) homogeneous and (b) heterogeneous dielectric substrates. (c)-(d) Upper and lower limits of the Coulomb modulation strength  $\lambda_{max}$  estimated from homogeneous and heterogeneous substrates for different  $\delta/h$  ratios and  $\varepsilon_{min}=3$ . (g) Example  $U_n$  profile corresponding to  $\tilde{U}=3\,\mathrm{eV},\ \lambda=0.25,\ \Omega=\phi=0.4\pi$  which could be realized with a patterned substrate as illustrated in the sketch below.

 $\delta$ , as depicted in Fig. 4 a). Note, that this kind of classical modeling can also be utilized in a multi-orbital scenario using the Wannier Function Continuum Electrostatics approach from Ref. 52. Here the screening effects of a homogeneous substrate can readily be calculated using the concept of image charges, as described in the Methods section. Doing so,  $U_n^{hom}$  is fully defined by the effective Wannier-orbital spread  $\delta$  and the dot-substrate separation h. In Fig. 4 a) we show a single  $U^{hom}(\varepsilon_{sub})$  for different  $\delta$  and h as a function of the substrate screening constant  $\varepsilon_{sub}$  and for a background  $\varepsilon_0 = 2$ . The unscreened (bare) value of the local Coulomb interaction is defined by  $\delta$ , whereas h controls its vulnerability to  $\varepsilon_{sub}$ . [53] We see that the local Coulomb interaction can be significantly modulated by changes to the homogeneous substrate screening.

As shown in the previous section, the key element of

our Coulomb-engineered topology proposal is, however, a spatial modulation of the local interactions  $U_n$ . To achieve this, we propose to spatially structure the substrate screening. A corresponding heterogeneous setup with just one dielectric interface in the substrate is depicted in Fig. 4 b). Here, we we approximate the resulting potential  $\Phi(\vec{x})$  with a multi-image-charge ansatz to fulfill the necessary boundary conditions (see Methods for more details). Fig. 4 b) shows a corresponding example in form of  $U^{het}(\varepsilon^L_{sub}, \varepsilon^R_{sub})$  for  $\delta/h=1$ . [54] We present data for  $\varepsilon^R_{sub}=\varepsilon^L_{sub}$  (homogeneous substrate),  $\varepsilon^R_{sub}=2$ , and  $\varepsilon^R_{sub}=10$ , from which we we see that the homogeneous solution smoothly interpolates between the two heterogeneous situations for  $\varepsilon_{sub}^L \in [2, 10]$ . As expected,  $U^{het}(\varepsilon_{sub}^L, \varepsilon_{sub}^R = 2)$  is always the largest due to the reduced screening from the right side of the substrate, while  $U^{het}(\varepsilon^L_{sub}, \varepsilon^R_{sub} = 10)$  is the smallest for  $\varepsilon_{sub}^L \in [2, 10]$ . Most importantly, we find that there are just minor quantitative changes to the local Coulomb interaction screened by  $\varepsilon^L_{sub}$  with  $\varepsilon^R_{sub}$  being different in the close vicinity. We can thus conclude that periodically patterned substrate screening functions with additional dielectric interfaces will not qualitatively affect the local substrate screening properties from the immediate surrounding.

Estimate of the Coulomb Modulation Strength: As described above and shown in Fig. 3f), the topological gap in the spin spectral function is proportional to  $t^2\lambda/U$ . The Coulomb modulation strength  $\lambda$  thus plays a significant role for our proposal as it maximizes the topological gap and thus protects the topological character of the system against perturbations. To estimate the maximal possible modulation strength we set  $\Omega$  and  $\phi$  to 0 in Eq. 2 and define  $\lambda_{max} = \frac{U_{max}}{U_{ave}} - 1 = \frac{\Delta_U}{U_{ave}}$  with  $\Delta_U = U_{max} - U_{min}$  and  $U_{ave} = (U_{max} + U_{min})/2$ . I.e.,  $\lambda_{max}$  is defined by the the maximally and minimally achievable local interactions. For the homogeneous substrate we can calculate  $\lambda_{max}^{hom}$  by defining  $U_{max} = U^{hom}(\varepsilon_{min})$  and  $U_{min} = U^{hom}(\varepsilon_{max})$  with  $\varepsilon_{min} < \varepsilon_{max}$ . In Fig. 4 c) we show the resulting values for fixed  $\varepsilon_{min} = 3$ .  $\lambda_{max}^{hom}$ steadily increases with the dielectric contrast  $\Delta_{\varepsilon}$ , which is driven by the enhacement of  $\Delta_U$  (due to the reduction of  $U_{min}$ ) upon increasing  $\varepsilon_{max}$ . Additionally,  $\lambda_{max}^{hom}$ increases with the  $\delta/h$  ratio, which results from a decreased  $U_{ave}$  for increased  $\delta$  and the enhanced substratescreening vulnerability of  $U^{hom}$  upon decreasing h.  $\lambda_{max}^{hom}$ is thus maximized by a large dielectric contrasts and large  $\delta/h$  ratios.

These homogeneous  $\lambda_{max}^{hom}$  are, however, just upper limits. In a more realistic setting,  $U_{max}$  and  $U_{min}$  might result from a heterogeneous substrate with additional dielectric interfaces as depicted in the sketch of Fig. 4 e). To estimate  $\lambda_{max}^{het}$  in such a setting we imagine the transition from  $U_{max}$  to  $U_{min}$  taking place within three lattice sites and set  $U_{max} = U^{het}(\varepsilon_{min}, \varepsilon_{mid})$  and  $U_{min} = U^{het}(\varepsilon_{max}, \varepsilon_{mid})$  with  $\varepsilon_{mid} = \varepsilon_{min} + \Delta_{\varepsilon}/2$ . The

resulting values are shown in Fig. 4 d). Due to the additional dielectric interface in the substrate,  $\Delta_U$  is decreased so that  $\lambda_{max}^{het}$  is overall smaller than  $\lambda_{max}^{hom}$ , but behaves otherwise similar. For  $\delta=2$  Å (orange and red dots)  $\lambda_{max}^{het}$  represents the lower limit since the interface is positioned here at  $y_0=\delta=2$  Å. By increasing  $y_0$   $\lambda_{max}^{het}$  approaches the upper limit  $\lambda_{max}^{hom}$ . The optimal parameter regime to realize screening-induced many-body topology is thus defined by small QD heights h, large QD diameters  $\delta$ , large QD separations  $y_0$ , and large dielectric contrasts  $\Delta_{\varepsilon}$  to increase  $\lambda_{max}$  (and thus the topological gap).

Defining the Coulomb Modulation Period and Phase: One possibility to define  $\Omega$  and  $\phi$  is to discretize the substrate screening function according to the lattice spacing and to choose the piece-wise defined  $\varepsilon_n$  so that a cosinelike pattern is generated, as illustrated for  $\Omega = 0.4\pi$ and  $\phi = 0.4\pi$  in Fig. 4 d). Although it is certainly a non-trivial task to create such dielectric patterns, we expect that lithographic approaches, atomically controlled grown materials using epitaxy techniques, or moiré patterns are capable of doing so. Importantly, due to the topological protection of the induced non-trivial states, perturbations to this screening-induced  $U_n$  patterns by defects or impurities or from smeared-out dielectric interfaces in the structured substrate, will not affect the result. Thus, we expect the proposed screening-induced topological states to be rather stable.

Conclusions: We have demonstrated that topological states of matter can be induced by engineering the screening environment of an electronic system. Our proposal compares with conventional schemes that rely on engineering single-particle physics, demonstrating that engineered electronic interactions are a powerful complementary tool for exploring novel quantum states. Our Coulomb-engineered topological states can emerge from both situations, those which can be fully understood on a mean-field level and those which must be explained in a pure many-body framework. We verify our proposal with the help of exact numerical calculations based on mean-field models for the former, and many-body tensor network techniques for the latter. Finally, we find from approximate solutions of the Poisson equation in realistic settings that the substrate screening can be strong enough to observe the proposed screening-induced states in experiments. Our results put forward a new method to create topological states of matter based on engineered interactions, providing a stepping stone to exploit dielectric engineering to realize exotic quantum states and to bring many-body physics closer to the fascinating field of topology.

**Acknowledgements** We thank L. Muechler for fruitful discussions. J.L.L. acknowledges the computational resources provided by the Aalto Science-IT project.

## Methods:

Tensor Network: We exactly solve the many-body

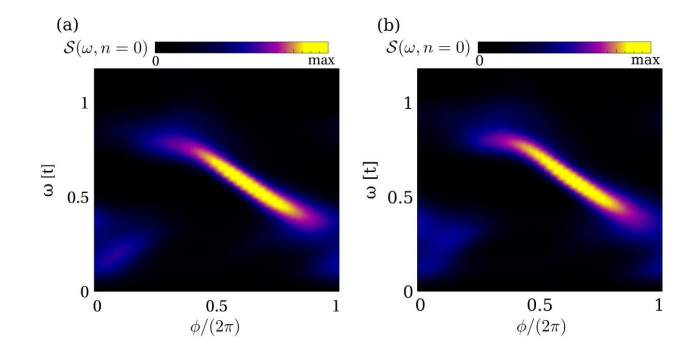


FIG. 5. Robustness of the edge modes: a) Spectral function of the edge for a finite second neighbor hopping, and b) with a finite random disorder in the local interactions, showing that the topological edge modes survive those perturbations. We took  $\tilde{U}=6t$  and  $\Omega=\pi/\sqrt{3}$ .

problems from the main text with the help of the kernel polynomial tensor network formalism.[55–60] Within the latter we expand the spectral function in terms of Chebyshev polynomials, whose coefficients can be efficiently computed using a recursion relation between tensor network wave functions.  $S(n,\omega)$  is subsequently represented in terms of N Chebyshev polynomials  $T_k(\omega)$ as  $S(\omega, n) = \frac{1}{\pi\sqrt{1-\omega^2}} \left(\mu_0 + 2\sum_{k=1}^N \mu_k T_k(\omega)\right)$ . The coefficients  $\mu_k$  are defined by  $\mu_k = \langle GS|S_n^z T_k(H)S_n^z|GS\rangle$ , which can be efficiently computed using the Chebyshev recursion relations. Once the first N/2 moments are computed, we use an autoregressive algorithm [61] to predict the next N/2 moments and reconstruct the spectral function using a Jackson kernel. [62] The autoregressive model halve the calculation costs and the Jackson kernel quenches Gibbs oscillations. This formalism allows to compute dynamical response functions of the many-body system directly in frequency space, without requiring any time evolution.

Robustness of the Edge Modes: Here we show how the topological edge modes are found to be robust against perturbations of the many-body Hamiltonian from Eq. 3. In particular we explore two different perturbations that are especially relevant for the experimental realization: second neighbor hopping and disorder in the interactions. First, the nearest neighbor hopping model from Eq. 3 is expected to be an approximation to the real system, as a finite overlap between second neighbor sites is expected. We capture this by adding a perturbation of the form  $H_{NNN}=t_{NNN}\sum_{n,s}c_{i,s}^{\dagger}c_{i+2,s}+h.c.$ . In Fig. 5 a) we show the spectral function at the edge under the influence of this additional perturbation for  $t_{NNN} = 0.1t$ , showing that the in-gap modes survive. Second, as our proposal requires to engineer different dielectric environments for each dot, defects in the fabrication are expected giving rise to imperfect interaction profiles. This can be captured by adding to the Hamiltonian from Eq. 3 a term

of the form  $H_W = \sum_n W_n \left( c_{n,\uparrow}^\dagger c_{n,\uparrow} - \frac{1}{2} \right) \left( c_{n,\downarrow}^\dagger c_{n,\downarrow} - \frac{1}{2} \right)$  where  $W_n$  are site-dependent random numbers. We show in Fig. 5 b) the spectral function at the edge including this onsite Coulomb disorder for  $W_n \in (-0.3t, 0.3t)$ , showing that the in-gap edge modes again survive disorder. These results highlight the robustness of the edge modes towards perturbations that are likely to present in the experimental setup.

Poisson Solver: To calculate the substrate-screened local Coulomb interactions  $U_n = e\Phi(\delta)$  we use the concept of image charges. In the case of a simple homogeneous substrate, as depicted in Fig. 4 a), we can choose an ansatz of the form

$$\Phi(\vec{x}) = \begin{cases} \frac{1}{\varepsilon_0} \frac{q_{00}}{|\vec{q}_{00} - \vec{x}|} + \frac{1}{\varepsilon_0} \frac{q_{01}}{|\vec{q}_{01} - \vec{x}|} & \text{for } y \ge 0\\ \frac{1}{\varepsilon_{sub}} \frac{q_{11}}{|\vec{q}_{11} - \vec{x}|} & \text{for } y < 0 \end{cases}, \quad (4)$$

where  $q_{00}$  and  $\vec{q}_{00}$  are the charge and position of the source charge, and  $q_{01}$ ,  $q_{11}$ ,  $\vec{q}_{01}$ , and  $\vec{q}_{11}$  are the charges and positions of the image charges. This potential needs to solve the Poisson equation in each  $\varepsilon_i$  region, i.e.

$$\Delta\Phi(\vec{x}) = \begin{cases} \frac{\rho(\vec{x})}{\varepsilon_0} & \text{for } y \ge 0\\ 0 & \text{for } y < 0 \end{cases}, \tag{5}$$

where  $\rho(\vec{x})$  is the point-charge density of the source charge  $q_{00}$ , and must full fill the boundary conditions

$$\Phi(\vec{x}_{u^+}) = \Phi(\vec{x}_{u^-}) \tag{6}$$

$$\varepsilon_0 \frac{\partial \Phi(\vec{x}_{y^+})}{\partial u} = \varepsilon_{sub} \frac{\partial \Phi(\vec{x}_{y^-})}{\partial u} \tag{7}$$

at the dielectric interface defined by y=0. By exploiting the full rotational symmetry around the y-axis (through the source charge), we can readily fix  $\vec{q}_{01}$  to the y=0-plane mirrored position of  $\vec{q}_{00}$  and choose  $\vec{q}_{11}=\vec{q}_{00}$ . Subsequently  $q_{01}$  and  $q_{11}$  are fixed by the boundary conditions yielding

$$q_{01} = \frac{\varepsilon_0 - \varepsilon_{sub}}{\varepsilon_0 + \varepsilon_{sub}} q_{00}, \tag{8}$$

$$q_{11} = q_{01} - q_{00}. (9)$$

Thus, in the case of a homogeneous substrate the influence of  $\varepsilon_{sub}$  to the local Coulomb interaction  $U_n$  can be calculated analytically. As soon as there is an additional dielectric interface in the substrate, as in the heterogeneous case depicted in Fig. 4 b), we cannot find an analytic solution any more. In order to estimate the impact of this heterogeneous substrate screening, we construct an approximate solution from a multiple image charge ansatz of the form

$$\Phi(\vec{x}) = \begin{cases}
\frac{1}{\varepsilon_0} \frac{q_{00}}{|\vec{q}_{00} - \vec{x}|} + \frac{1}{\varepsilon_0} \sum_{i}^{2N} \frac{q_{0i}}{|\vec{q}_{0i} - \vec{x}|} , y \ge 0 \\
\frac{1}{\varepsilon_{sub}^L} \sum_{i}^{N} \frac{q_{1i}}{|\vec{q}_{1i} - \vec{x}|} , y < 0, x \le 0 \\
\frac{1}{\varepsilon_{sub}^R} \sum_{i}^{N} \frac{q_{2i}}{|\vec{q}_{2i} - \vec{x}|} , y < 0, x > 0
\end{cases} (10)$$

which is supposed to solve the Poisson equation given in Eq. (5) with the boundary conditions at the y=0 interfaces

$$\Phi(\vec{x}_{v^{+}}) = \Phi(\vec{x}_{v^{-}}) \qquad y = 0 \tag{11}$$

$$\varepsilon_0 \frac{\partial \Phi(\vec{x}_{y^+})}{\partial y} = \varepsilon_{sub}^L \frac{\partial \Phi(\vec{x}_{y^-})}{\partial y} \qquad y = 0, x \le 0$$
 (12)

$$\varepsilon_0 \frac{\partial \Phi(\vec{x}_{y^+})}{\partial y} = \varepsilon_{sub}^R \frac{\partial \Phi(\vec{x}_{y^-})}{\partial y} \qquad y = 0, x > 0$$
 (13)

and at the x = 0 interface in the substrate

$$\Phi(\vec{x}_{x^+}) = \Phi(\vec{x}_{x^-}) \qquad y < 0, x = 0 \tag{14}$$

$$\varepsilon_{sub}^{L} \frac{\partial \Phi(\vec{x}_{x^{+}})}{\partial x} = \varepsilon_{sub}^{R} \frac{\partial \Phi(\vec{x}_{x^{-}})}{\partial x} \qquad y < 0, x = 0.$$
 (15)

If we fix all image charge positions we can use the 4N image charges  $q_{(0,1,2)i}$  to fulfill 4N boundary conditions at discrete interface positions  $\vec{x}_i$ . The resulting linear equation system is well defined and has a unique solution. Here, however, we reformulate the Poisson equation into a minimization problem of the form

$$\min_{q_{(0,1,2)i}} \left\| \begin{array}{cc} \Delta\Phi(\vec{x}) - \frac{\rho(\vec{x})}{\varepsilon_0} & \text{for } y \ge 0.0 \\ \Delta\Phi(\vec{x}) & \text{for } y < 0.0 \end{array} \right\|, \tag{16}$$

using the boundary conditions from Eqs. (11-15) to define constraints for the minimization. This relaxes the one-to-one correspondence between the number of image charges and the number of discrete boundary conditions.

Numerically, we use the Sequential Least SQuares Programming (SLSQP) algorithm [63] as implemented in the Scipy minimization package. We use  $5 \times 2 \times 5$  image charges per substrate region (i.e. 100 in total), separated by  $(d_x, d_y, d_z) = (4, 4, 4)$  Å and distributed as indicated in Fig. 6, and 182 boundary condition points at the y=0interface and 130 points at the x = 0 interface distributed as also indicated in Fig. 6. To minimize the function defined in Eq. (16) we evaluate the Poisson equation on a discrete grid of 18 points in the x/z plane slightly below the source charge (see Fig. 6). The source charge is positioned at  $\vec{q}_{00} = (h, y_0 = -2, 0)$  (with variable distance h to the y=0 interface and fixed position relative to the vertical interface in the substrate) and its potential is approximated using a three-dimensional Gauss function of the form

$$\rho(\vec{x}) = \frac{q_{00}}{\sigma^3 (2\pi)^{3/2}} \exp\left(-\frac{(\vec{q}_{00} - \vec{x})^2}{\sigma^2}\right)$$
(17)

with  $\sigma = 0.15$  Å. Finally,  $U_n = e\Phi(\vec{\delta})$  is evaluated using  $eq_{00} \approx 14.39 \,\text{eV}$ Å and  $\vec{\delta} = \vec{q}_{00} + (\delta, 0, 0)$  with variable  $\delta$ .

In Fig. 6 we show a corresponding example result for  $\varepsilon_0=2$ ,  $\varepsilon_{sub}^L=4$ ,  $\varepsilon_{sub}^R=10$ ,  $h=2\,\text{Å}$ , and  $\delta=|y_0|=2\,\text{Å}$ . In this situation we would a priori expect to see equipotential lines with small kinks at the  $\varepsilon_0/\varepsilon_{sub}^L$  boundary and with enhanced kinks at the interfaces to the  $\varepsilon_{sub}^R$ 

area, which is approximately the case in our numerical estimate. Furthermore, we see that these boundary conditions are also approximately full filled between the discrete boundary positions in the vicinity of the source charge (red dot). Further away, we, however, also find deviations to this. We thus expect our numerical solution to by approximately valid in the vicinity of the source charge, which is enough to estimate the local Coulomb interaction.

As an important benchmark for the chosen numerical parameters and as a sanity check, we need to reproduce the analytical potential in the case of a homogeneous substrate, i.e.  $\varepsilon^L_{sub} = \varepsilon^R_{sub}$ , which is approximately the case as we can see from Fig. 4 b) at  $\varepsilon^R_{sub} = 2$  (dotted line) and  $\varepsilon^R_{sub} = 10$  (dashed line).

- [1] X.-L. Qi and S.-C. Zhang, Rev. Mod. Phys. 83, 1057 (2011).
- [2] M. Z. Hasan and C. L. Kane, Rev. Mod. Phys. 82, 3045 (2010).
- [3] Y. Ando, Journal of the Physical Society of Japan 82, 102001 (2013).
- [4] C. L. Kane and E. J. Mele, Phys. Rev. Lett. 95, 226801 (2005).
- [5] C. Beenakker, Annual Review of Condensed Matter Physics 4, 113 (2013).
- [6] V. Mourik, K. Zuo, S. M. Frolov, S. R. Plissard, E. P. A. M. Bakkers, and L. P. Kouwenhoven, Science 336, 1003 (2012).
- [7] S. Nadj-Perge, I. K. Drozdov, J. Li, H. Chen, S. Jeon, J. Seo, A. H. MacDonald, B. A. Bernevig, and A. Yazdani, Science 346, 602 (2014).
- [8] L. Fu, Phys. Rev. Lett. **106**, 106802 (2011).
- [9] Y. Tanaka, Z. Ren, T. Sato, K. Nakayama, S. Souma, T. Takahashi, K. Segawa, and Y. Ando, Nature Physics 8, 800 (2012).
- [10] J. Seidel, Nature Materials 18, 188 (2019).
- [11] L. Šmejkal, Y. Mokrousov, B. Yan, and A. H. MacDonald, Nature Physics 14, 242 (2018).
- [12] J. Alicea, Y. Oreg, G. Refael, F. von Oppen, and M. P. A. Fisher, Nature Physics 7, 412 (2011).
- [13] F. Schindler, A. M. Cook, M. G. Vergniory, Z. Wang, S. S. P. Parkin, B. A. Bernevig, and T. Neupert, Science Advances 4, eaat0346 (2018).
- [14] F. Schindler, Z. Wang, M. G. Vergniory, A. M. Cook, A. Murani, S. Sengupta, A. Y. Kasumov, R. Deblock, S. Jeon, I. Drozdov, H. Bouchiat, S. Guéron, A. Yazdani, B. A. Bernevig, and T. Neupert, Nature Physics 14, 918 (2018).
- [15] Z. Gong, Y. Ashida, K. Kawabata, K. Takasan, S. Hi-gashikawa, and M. Ueda, Phys. Rev. X 8, 031079 (2018).
- [16] H. Shen, B. Zhen, and L. Fu, Phys. Rev. Lett. 120, 146402 (2018).
- [17] M. M. Denner, A. Skurativska, F. Schindler, M. H. Fischer, R. Thomale, T. Bzdušek, and T. Neupert, arXiv e-prints, arXiv:2008.01090 (2020), arXiv:2008.01090 [cond-mat.mes-hall].
- [18] H. C. Po, H. Watanabe, and A. Vishwanath, Phys. Rev.

- Lett. 121, 126402 (2018).
- [19] J. Ahn, S. Park, and B.-J. Yang, Phys. Rev. X 9, 021013 (2019).
- [20] Y. E. Kraus and O. Zilberberg, Nature Physics 12, 624 (2016).
- [21] Y. E. Kraus, Y. Lahini, Z. Ringel, M. Verbin, and O. Zilberberg, Phys. Rev. Lett. 109, 106402 (2012).
- [22] A. Agarwala and V. B. Shenoy, Phys. Rev. Lett. 118, 236402 (2017).
- [23] K. Pöyhönen, I. Sahlberg, A. Westström, and T. Ojanen, Nature Communications 9 (2018), 10.1038/s41467-018-04532-x.
- [24] E. Dagotto, Rev. Mod. Phys. **66**, 763 (1994).
- [25] J. K. Jain, Phys. Rev. Lett. 63, 199 (1989).
- [26] R. Willett, J. P. Eisenstein, H. L. Störmer, D. C. Tsui, A. C. Gossard, and J. H. English, Phys. Rev. Lett. 59, 1776 (1987).
- [27] S. Raghu, X.-L. Qi, C. Honerkamp, and S.-C. Zhang, Phys. Rev. Lett. 100, 156401 (2008).
- [28] M. Dzero, K. Sun, V. Galitski, and P. Coleman, Phys. Rev. Lett. 104, 106408 (2010).
- [29] M. Dzero, J. Xia, V. Galitski, and P. Coleman, Annual Review of Condensed Matter Physics 7, 249 (2016).
- [30] W. Chen and J. L. Lado, Phys. Rev. Lett. 122, 016803 (2019).
- [31] M. Rösner, C. Steinke, M. Lorke, C. Gies, F. Jahnke, and T. O. Wehling, Nano Letters 16, 2322 (2016), publisher: American Chemical Society.
- [32] A. Raja, A. Chaves, J. Yu, G. Arefe, H. M. Hill, A. F. Rigosi, T. C. Berkelbach, P. Nagler, C. Schüller, T. Korn, C. Nuckolls, J. Hone, L. E. Brus, T. F. Heinz, D. R. Reichman, and A. Chernikov, Nature Communications 8, 15251 (2017), number: 1 Publisher: Nature Publishing Group.
- [33] M. I. B. Utama, H. Kleemann, W. Zhao, C. S. Ong, F. H. da Jornada, D. Y. Qiu, H. Cai, H. Li, R. Kou, S. Zhao, S. Wang, K. Watanabe, T. Taniguchi, S. Tongay, A. Zettl, S. G. Louie, and F. Wang, Nature Electronics 2, 60 (2019), number: 2 Publisher: Nature Publishing Group.
- [34] L. Waldecker, A. Raja, M. Rösner, C. Steinke, A. Bostwick, R. J. Koch, C. Jozwiak, T. Taniguchi, K. Watanabe, E. Rotenberg, T. O. Wehling, and T. F. Heinz, Physical Review Letters 123, 206403 (2019), publisher: American Physical Society.
- [35] P. G. Harper, Proceedings of the Physical Society. Section A 68, 874 (1955).
- [36] S. Aubry and G. André (1980).
- [37] D. J. Thouless, M. Kohmoto, M. P. Nightingale, and M. den Nijs, Phys. Rev. Lett. 49, 405 (1982).
- [38] D. J. Thouless, Phys. Rev. B 27, 6083 (1983).
- [39] I. Petrides and O. Zilberberg, Phys. Rev. Research 2, 022049 (2020).
- [40] A. Spinelli, B. Bryant, F. Delgado, J. Fernández-Rossier, and A. F. Otte, Nature Materials 13, 782 (2014).
- [41] We take  $\lambda \ll 1$  and  $\Omega \ll 1$ .
- [42] J. L. Lado and O. Zilberberg, Phys. Rev. Research 1, 033009 (2019).
- [43] U. Agrawal, S. Gopalakrishnan, and R. Vasseur, Nature Communications 11 (2020), 10.1038/s41467-020-15760-5.
- [44] L. Savary and L. Balents, Reports on Progress in Physics 80, 016502 (2016).
- [45] We assume in the mean field ansatz that time reversal

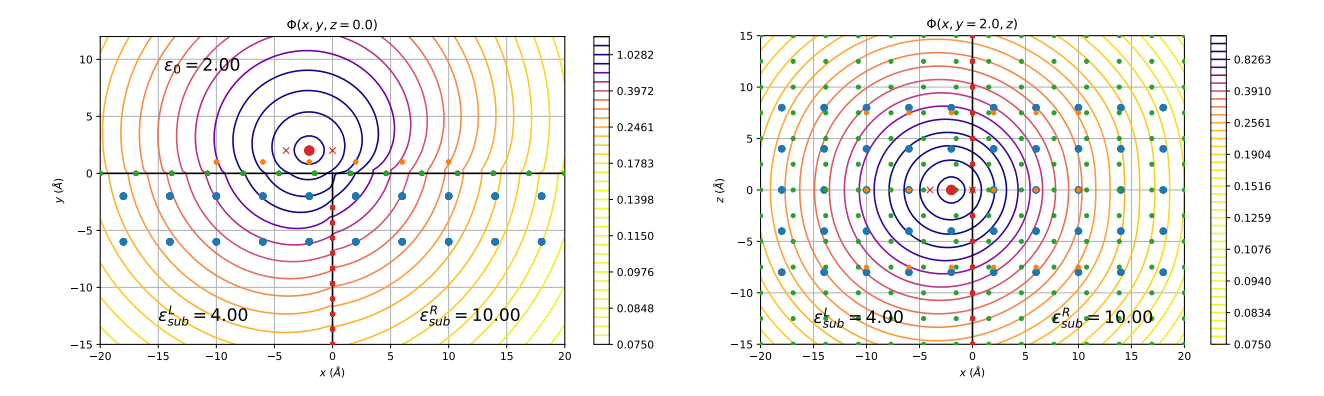


FIG. 6. Example Result of the Multi-Image-Charge Approach. Left and right show the numerically evaluated potential for  $\varepsilon_0 = 2$ ,  $\varepsilon_{sub}^L = 4$ ,  $\varepsilon_{sub}^R = 10$ , h = 2 Å, and  $\delta = y_0 = 2$  Å in the (x,y) and (x,z) planes. Red dot: Source charge position, orange dots: Poisson equation evaluation points, green dots: y = 0 interface discrete boundary condition points, red dots: x = 0 interface discrete boundary condition points, blue dots: image charge positions, black lines: dielectric interfaces.

- symmetry is not broken and that no anomalous terms are generated, as will be expected for the uniform Heisenberg model.
- [46] J. R. Krenn, A. Dereux, J. C. Weeber, E. Bourillot, Y. Lacroute, J. P. Goudonnet, G. Schider, W. Gotschy, A. Leitner, F. R. Aussenegg, and C. Girard, Physical Review Letters 82, 2590 (1999), publisher: American Physical Society.
- [47] S. A. Maier, M. L. Brongersma, P. G. Kik, and H. A. Atwater, Physical Review B 65, 193408 (2002), publisher: American Physical Society.
- [48] J. H. Lee, Z. M. Wang, B. L. Liang, W. T. Black, V. P. Kunets, Y. I. Mazur, and G. J. Salamo, Nanotechnology 17, 2275 (2006), publisher: IOP Publishing.
- [49] V. P. Kunets, M. Rebello Sousa Dias, T. Rembert, M. E. Ware, Y. I. Mazur, V. Lopez-Richard, H. A. Mantooth, G. E. Marques, and G. J. Salamo, Journal of Applied Physics 113, 183709 (2013), publisher: American Institute of Physics.
- [50] H. Kim, A. Palacio-Morales, T. Posske, L. Rózsa, K. Palotás, L. Szunyogh, M. Thorwart, and R. Wiesendanger, Science Advances 4, eaar5251 (2018), publisher: American Association for the Advancement of Science Section: Research Article.
- [51] A. Kamlapure, L. Cornils, J. Wiebe, and R. Wiesendanger, Nature Communications 9, 3253 (2018), number: 1

- Publisher: Nature Publishing Group.
- [52] M. Rösner, E. Şaşıoğlu, C. Friedrich, S. Blügel, and T. O. Wehling, Physical Review B 92, 085102 (2015), publisher: American Physical Society.
- [53] Systems with a small Wannier-orbital spread  $\delta$  have large local Coulomb interactions, and systems with small effective heights h are more strongly effected by the substrate.
- [54] We assume the location of the source charge above  $\varepsilon_{sub}^L$  as also depicted in the sketch of Fig. 4 b).
- [55] A. Weiße, G. Wellein, A. Alvermann, and H. Fehske, Rev. Mod. Phys. 78, 275 (2006).
- [56] F. A. Wolf, J. A. Justiniano, I. P. McCulloch, and U. Schollwöck, Phys. Rev. B 91, 115144 (2015).
- [57] J. L. Lado and M. Sigrist, Phys. Rev. Research 2, 023347 (2020).
- [58] ITensor Library http://itensor.org.
- [59] M. Fishman, S. R. White, and E. Miles Stoudenmire, arXiv e-prints , arXiv:2007.14822 (2020), arXiv:2007.14822 [cs.MS].
- [60] DMRGpy Library https://github.com/joselado/dmrgpy.
- [61] H. Akaike, Annals of the Institute of Statistical Mathematics 21, 243 (1969).
- [62] D. Jackson, Transactions of the American Mathematical Society 13, 491 (1912).
- [63] D. Kraft, A software package for sequential quadratic programming, Tech. Rep. (Institute for Flight Mechanics, Koln, Germany, 1988).